Structural Analysis and Testing of the Inflatable Re-entry Vehicle Experiment (IRVE)

Michael C. Lindell* and Stephen J. Hughes†
NASA Langley Research Center, Hampton, VA, 23681

Megan Dixon‡ and Cliff E. Willey§
ILC Dover LP, Frederica, DE, 19946

The Inflatable Re-entry Vehicle Experiment (IRVE) is a 3.0 meter, 60 degree half-angle sphere cone, inflatable aeroshell experiment designed to demonstrate various aspects of inflatable technology during Earth re-entry. IRVE will be launched on a Terrier-Improved Orion sounding rocket from NASA's Wallops Flight Facility in the fall of 2006 to an altitude of approximately 164 kilometers and re-enter the Earth's atmosphere. The experiment will demonstrate exo-atmospheric inflation, inflatable structure leak performance throughout the flight regime, structural integrity under aerodynamic pressure and associated deceleration loads, thermal protection system performance, and aerodynamic stability. Structural integrity and dynamic response of the inflatable will be monitored with photogrammetric measurements of the leeward side of the aeroshell during flight. Aerodynamic stability and drag performance will be verified with on-board inertial measurements and radar tracking from multiple ground radar stations. In addition to demonstrating inflatable technology, IRVE will help validate structural, aerothermal, and trajectory modeling and analysis techniques for the inflatable aeroshell system. This paper discusses the structural analysis and testing of the IRVE inflatable structure. Equations are presented for calculating fabric loads in sphere cone aeroshells, and finite element results are presented which validate the equations. Fabric material properties and testing are discussed along with aeroshell fabrication techniques. Stiffness and dynamics tests conducted on a small-scale development unit and a full-scale prototype unit are presented along with correlated finite element models to predict the in-flight fundamental mode.

Nomenclature

α	=	sphere cone angle
D_A	=	aeroshell diameter
D_C	=	centerbody diameter
D_T	=	toroid diameter
H_S	=	height of spar fabric
m_c	=	mass of centerbody
N_{MAX}	=	fabric running load
P	=	inflation pressure
q	=	aerodynamic surface pressure
W_S	=	width of spar fabric spacing between toroids

* IRVE Structural Analyst, Structural & Thermal Systems Branch, NASA LaRC/MS431, AIAA Member.
† IRVE Lead Design Engineer, Mechanical Systems Branch, NASA LaRC/MS432, AIAA Member.
‡ Design Engineer, ILC Dover Engineered Inflatables, One Moonwalker Rd/MS22, Frederica, DE 19946, AIAA Member.
§ Program Manager, Space Inflatables, ILC Dover LP, One Moonwalker Rd/MS32, Frederica, DE 19946, AIAA Senior Member.

I. Introduction

LIGHTWEIGHT inflatable aeroshells are being investigated as a means of atmospheric entry for science payloads returning from the International Space Station, the Moon, and Mars. Inflatable aeroshells offer several advantages over traditional rigid aeroshells for atmospheric entry. These structures can be stowed in existing (and relatively small) Expendable Launch Vehicles, offering increased payload volume fraction within the launch vehicle shroud, and can be deployed to very large diameters (20 to 30 meters). A very large surface to mass ratio can be achieved resulting in a significant reduction in aero-heating. Inflatable aeroshells offer the potential to deliver more payload mass to the surface for equivalent trajectory constraints. Existing materials can be used in most inflatable aeroshell applications, not requiring radical leaps in material technology. Propellant reductions are possible with low volume and lightweight inflatable structures, reducing the propellant requirements leaving Earth and also reducing fuel consumption during the aerobraking maneuver on the return to Earth.

There are, however, several technical challenges for inflatable aeroshells. The fact that inflatable aeroshells are flexible structures could lead to unpredictable drag performance or aero-structural dynamic instability. High pressure needs to be maintained inside the inflatables to maintain shape and to react aerodynamic forces. Inflatables will have some level of gas leakage and, depending on the rate, require a make-up gas source. Also, aerothermal heating during planetary entry poses a material challenge. Multiple thermal protection layers with high temperature capability are required which can account for a significant part of the system mass.

The structural analysis and testing of the IRVE inflatable structure are the focus of this paper. Pertinent design and fabrication details will also be given. Structural analysis of the inflatable involves both closed-form equations and finite element analyses. The peak structural loads on the fabric structures can be obtained with sufficient accuracy by force equilibrium equations. Design equations are presented to allow quick sizing of similarly constructed inflatable sphere cone aeroshells. Closed-form results are compared with results from finite element analyses. Finite element analyses of thin-fabric aeroshells present a challenge in that both material and geometric nonlinearities arise due to the nonlinear load/deflection behavior of the fabric (at low loads), pressure stiffening of the inflated fabric, fabric-to-fabric contact between the inflated fabric and the aeroshell surface, and fabric wrinkling on the aeroshell surface. In addition to checking fabric loads, the finite element model is used to predict the fundamental mode of the aeroshell system.

A variety of tests are involved in gaining confidence in the inflatable aeroshell. Material tests have been performed to characterize the fabric load/deflection behavior and the fabric breaking strength, and strength tests have been performed to characterize the fabric seams. A two-cell demonstration test unit was fabricated and tested to validate fabrication techniques and measure leak performance, strength, and dynamics. A full-scale prototype unit was also built and tested in a vacuum chamber at NASA Langley Research Center to test packing and deployment, and to measure leak rates and survey system modes. The modal survey was used to validate the stiffness of the finite element model which was then used to predict the in-flight fundamental mode of the aeroshell. The fundamental mode of the inflated aeroshell must be sufficiently above the expected aerodynamic excitations to avoid coupling and potential aerodynamic instability.

II. Mission Concept

IRVE will launch out of NASA's Wallops Flight Facility on a Terrier-Improved Orion sounding rocket. Second stage ignition occurs at 15 seconds into the flight with burnout at 40 seconds. The vehicle coasts for another 20 seconds after burnout to an altitude of 71 km at which point the IRVE, telemetry module, and nosecone eject from the spent second stage. After another 20 seconds (80 seconds into the flight) the IRVE separates from the telemetry module/nosecone assembly. Apogee is reached at 201 seconds into the flight at an altitude of 164 km. At 210 seconds IRVE inflation begins and the aeroshell shape is attained prior to encountering the atmospheric interface. Full inflation pressure is achieved at 325 seconds and an altitude of 93 km. The vehicle passes through the peak dynamic pressure at 364 seconds at an altitude of 46 km and a Mach number of 2.56. The experiment is officially concluded after that point. Water impact occurs at 1120 seconds. The mission concept is shown graphically in Fig. 1.

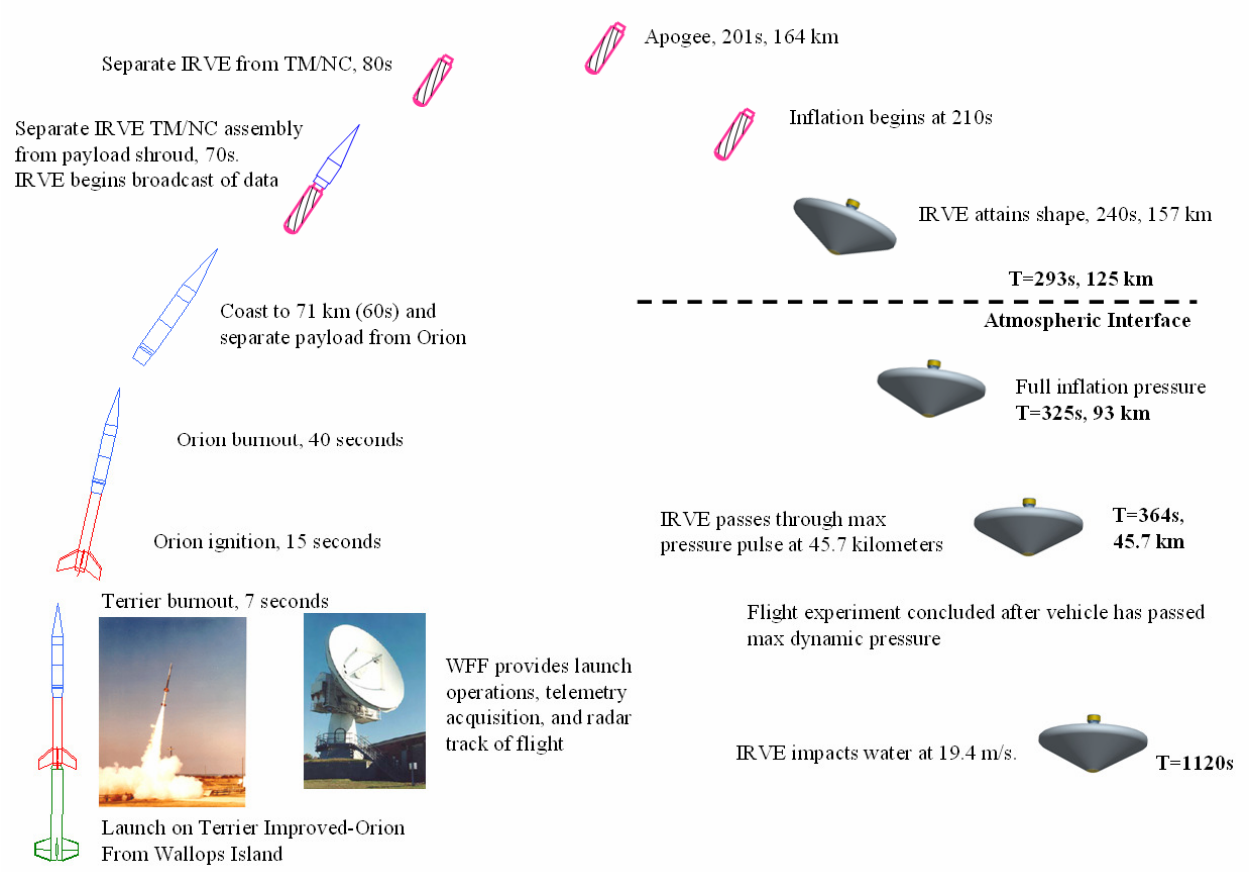

Figure 1. IRVE mission concept.

III. System Design

The design of the IRVE system (Fig. 2) consists of the centerbody structure, which houses the electronics and inflation subsystems, and the inflatable aeroshell. The diameter of the inflated system is 3.0 meters and the height is approximately 1.6 meters.

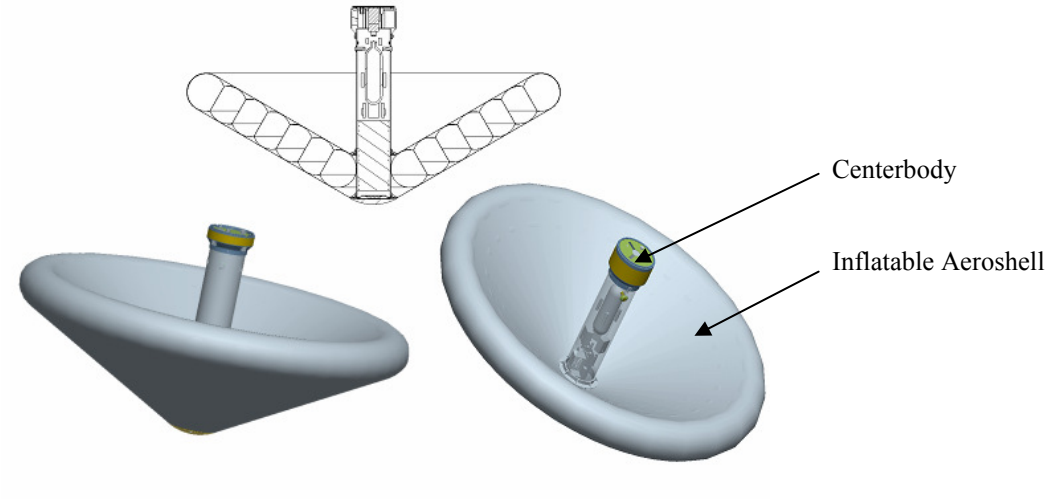

Figure 2. IRVE system.

A. Centerbody Structure

The centerbody structure consists of a 10.75-inch diameter aluminum tube that supports the electronics and inflation subsystems, a Teflon nose cap, a vehicle interface ring that attaches IRVE to the launch vehicle, and two attachment rings that tie the aeroshell fabric to the centerbody. The centerbody components are shown in Fig. 3. The highest loads on the centerbody structure and subsystems, with the exception of the fabric attachment rings, occur at launch and are directed along the launch axis. The centerbody subsystems were designed to withstand an axial load of approximately 50g, primarily driven by random vibration. The fabric attachment rings experience their highest loads during re-entry at maximum dynamic pressure when the fabric aeroshell is decelerating the vehicle.

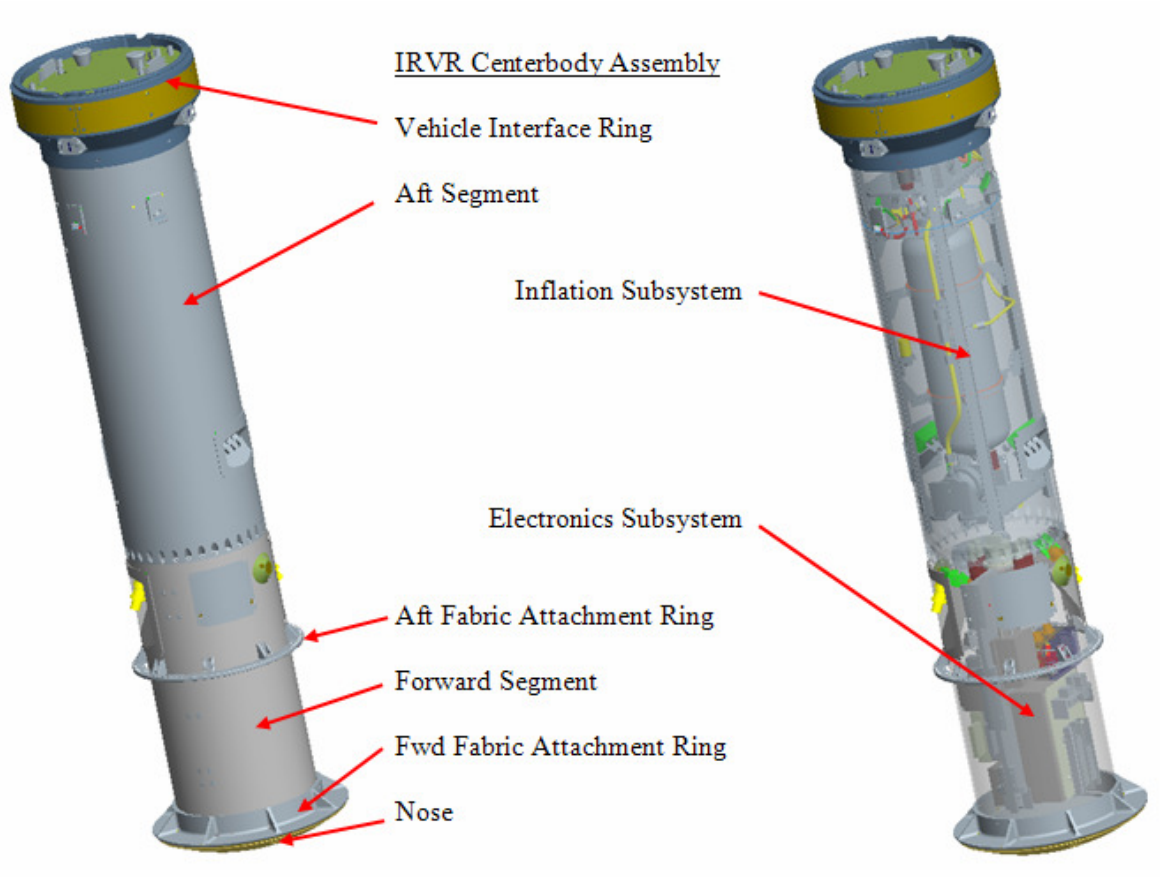

Figure 3. Centerbody components.

B. Inflatable Aeroshell

A cross-section of the IRVE system is shown in Fig. 4. The inflatable aeroshell consists of seven toroids arranged into three separate inflatable volumes which are laced together and contained within a restraint wrap. The inflatable volumes or bladders are made of a silicone coated Kevlar fabric. The restraint wrap consists of dry Kevlar fabric for the structural loads, layers of Nextel 312 cloth for thermal protection, and Kapton layers to act as a gas barrier. The material layup is shown in Fig. 5.

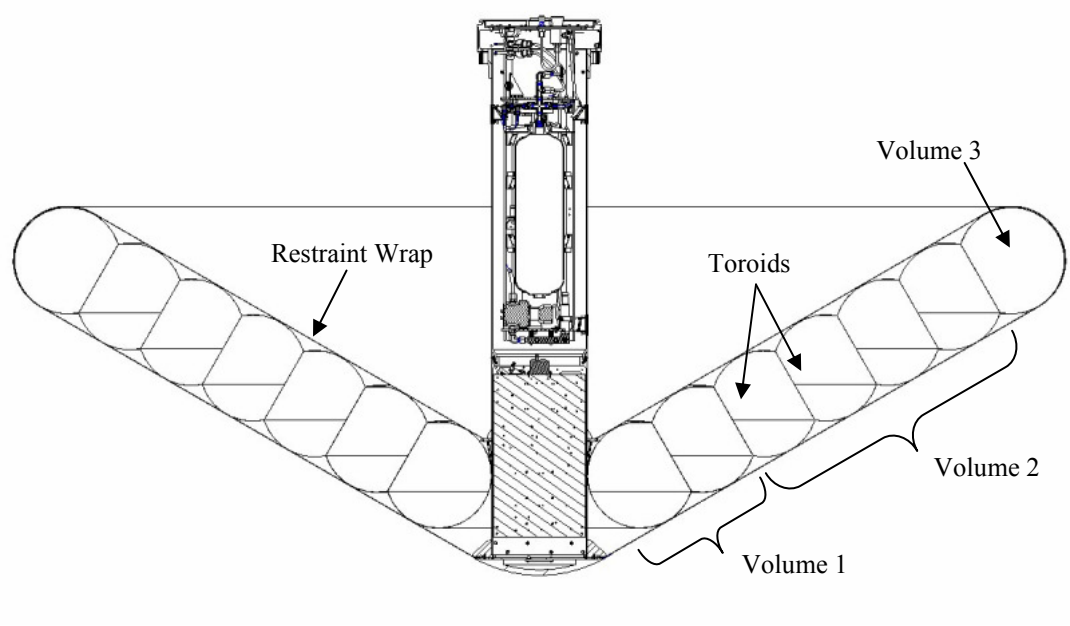

Figure 4. IRVE cross-section.

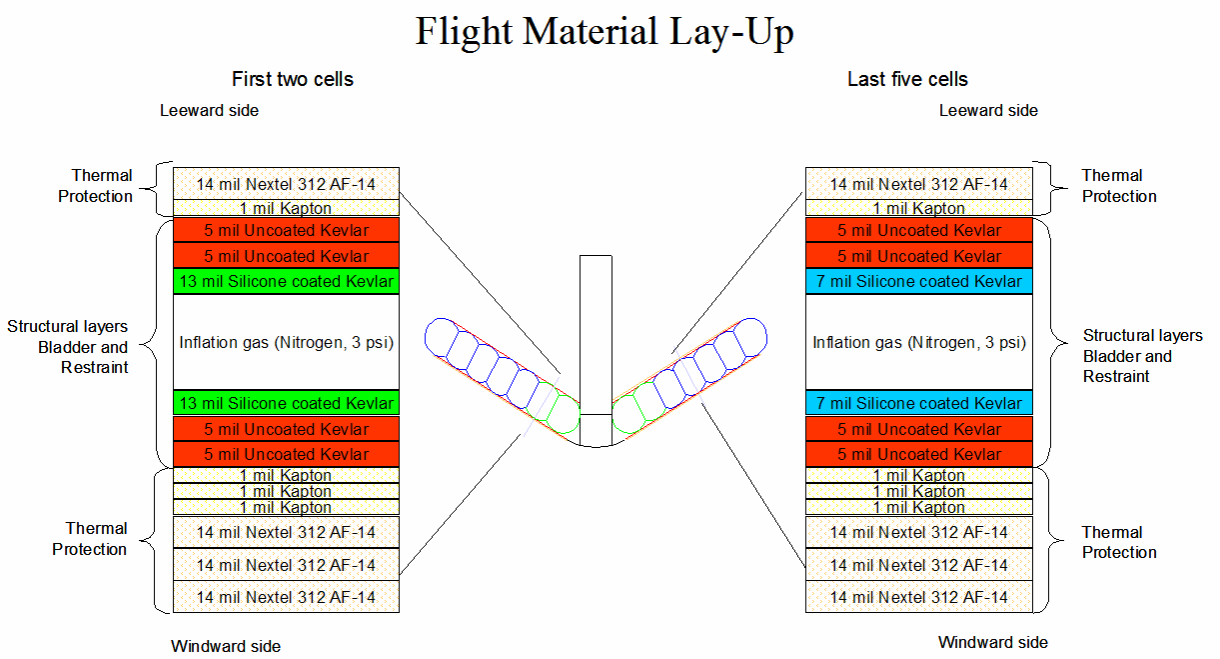

Figure 5. Inflatable structure material layup.

IV. Inflatable Aeroshell Analysis

The structural analysis of the inflatable consists of both closed-form equations and finite element analyses. Finite element analyses were used to verify the closed-form equations and to predict the fundamental mode of the system during free flight.

A. Aeroshell Loads

The loads on the inflatable structure come from internal inflation pressure and from the dynamic pressure of re-entry (and associated deceleration). The nominal design inflation pressure is 3.0 psi and the structure will be proof tested to 5.25 psi. The predicted maximum surface (stagnation) pressure is 0.22 psi resulting in a maximum deceleration of 7.7g.

B. Fabric Analysis

Using the sphere cone geometry of IRVE, several closed-form equations were developed to calculate the loads in the fabric structures of the inflatable aeroshell. These equations were validated against finite element models and found to be accurate for nominal load prediction. The general geometry of a sphere cone aeroshell is shown in Fig. 6. Loads on the various elements of the aeroshell can be derived from force equilibrium.

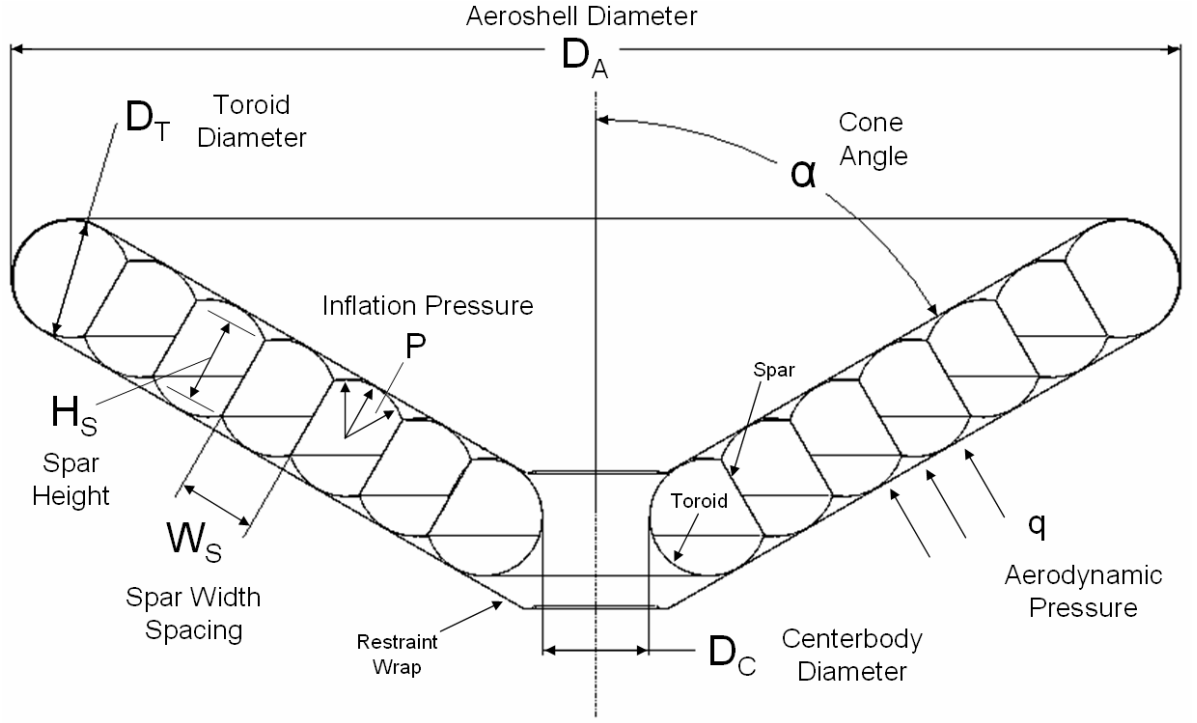

Figure 6. Sphere cone geometry.

1. Toroid Fabric Loads

The fabric load in the inflated toroids is dependent on the inflation pressure, the toroid diameter, and the centerbody diameter. The maximum load occurs at the inner radius of the inner toroid. The equation for the fabric running load (force per unit width) as a function of these parameters is given in Eq. (1).

$$N_{MAX} = \frac{PD_T}{4}\left[2 + \frac{D_T}{D_C}\right] \tag{1}$$

Using the design inflation pressure of 3.0 psi gives a maximum toroid fabric running load of 27.9 lbs/in. It should be noted that the aerodynamic pressure does not appear in Eq. (1) and finite element analysis verified that aerodynamic pressure had an insignificant effect on the toroid running load.

2. Spar Fabric Loads

The spars are the fabric members that partition the individual toroid cells. Subject to inflation pressure, the maximum spar load occurs in the innermost spar at the spar end closest to the aeroshell axis of symmetry. The spar

fabric load is a function of the inflation pressure, the toroid diameter, the centerbody diameter, and the cone angle, and is given by Eq. (2).

$$N_{MAX} = \frac{PW_S}{2}\left[1 + \frac{1}{1 - \dfrac{H_S \cos(\alpha)}{D_C + D_T + W_S \sin(\alpha)}}\right] \approx PW_S \tag{2}$$

Given the geometry of the IRVE design, the maximum spar fabric running load is 26.1 lbs/in. As with Eq. (1), the aerodynamic pressure has an insignificant effect on the spar running load and does not appear in Eq. (2). Equation (2) assumes continuous spars circumferentially. In reality the spars are segmented into 16 sections with 0.5-inch wide gaps in between to span the bladder seams. Based on experience with IRVE, a good design value for the spar loads is 2.5 times the value given by Eq. (2) due to stress concentrations from the spar discontinuities and manufacturing tolerances on the spar lengths (heights).

3. Restraint Wrap Loads

The loads in the restraint wrap are driven by the aerodynamic pressure and the associated deceleration of the system. The maximum loads occur at the fabric/centerbody interface where the running length of fabric is the smallest. Assuming that the load is equally shared between the forward and aft restraint wrap interfaces, and neglecting the pressure on the nose of the centerbody, force equilibrium on the centerbody gives the restraint wrap running load as a function of the mass of the centerbody, the deceleration, the diameter of the centerbody, and the cone angle as given in Eq. (3).

$$N_{MAX} = \frac{m_C a}{2\pi D_C \cos(\alpha)} \tag{3}$$

An equivalent equation was derived in terms of the aerodynamic pressure by using force equilibrium on the inflatable aeroshell (without the centerbody) but Eq. (3) is simpler to use. The weight of the centerbody for IRVE is approximately 150 lbs and the peak deceleration during re-entry, at maximum dynamic pressure, is 7.7g. Instead of using the centerbody diameter of 10.75 inches for D_C, a larger value is more accurate because the attachment rings interface to the fabric at a larger diameter than the centerbody tube. The two rings are about an inch different in diameter, the average diameter being about 14.8 inches. Therefore, using a 14.8-inch diameter, the maximum running load in the restraint wrap fabric at the attachments to the centerbody is 24.8 lbs/in.

4. Finite Element Comparison

Equations (1) through (3) were checked against finite element analysis results for IRVE as well as for a number of different aeroshell sizes (up to 30 meters). The applied loads were internal inflation pressure, external surface pressure, and inertia relief due to the deceleration. The analysis was performed using MSC.Nastran nonlinear solution sequence 106. Nonlinear analysis is required to capture the load stiffening effect on thin fabrics. The nonlinearity of the fabric material properties (load/deflection curves) was not modeled but rather the orthotropic properties were adjusted to correlate with stiffness test data near the flight load condition. Another source of nonlinearity arises from fabric-to-fabric contact between the inflated toroids and the restraint wrap. The restraint wrap fabric is only attached to the toroids at the outer diameter of the outer toroid and contacts the remaining toroids at the tangency points. The contact effect was investigated using MSC.Marc and compared with results from an analysis in MSC.Nastran where contact was not modeled and the tangency points were connected. The difference in dynamics between the two models, as measured by the fundamental frequency, was about 10%. Since the difference was not large and the run time for the MSC.Nastran model without contact was significantly shorter, the MSC.Nastran model was used for further analysis.

Fig. 7 shows the finite element model of the IRVE system. The meridional shell force resultants for the toroids and spars under the flight load condition are shown in Fig. 8. Figure 9 shows the meridional shell force resultants in the restraint wrap. Equations (1) through (3) compared well the finite element results as shown in Table 1.

Table 1. Finite element results vs. closed-form results

Fabric Location	Finite Element	Closed-form (Eq.)	% Difference
Toroid	28.4 lbs/in	27.9 lbs/in (1)	-1.8
Spar	26.8 lbs/in	26.1 lbs/in (2)	-2.6
Restraint Wrap Fwd	22.0 lbs/in	24.8 lbs/in (3)	12.7
Restraint Wrap Aft	28.7 lbs/in	24.8 lbs/in (3)	-13.6

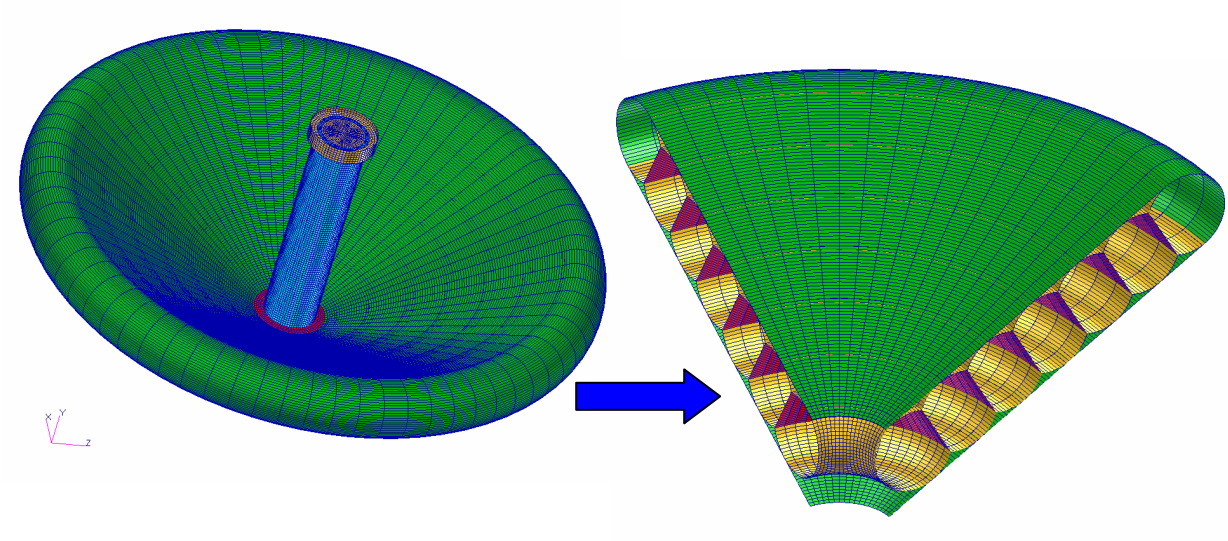

Figure 7. Deployed finite element model.

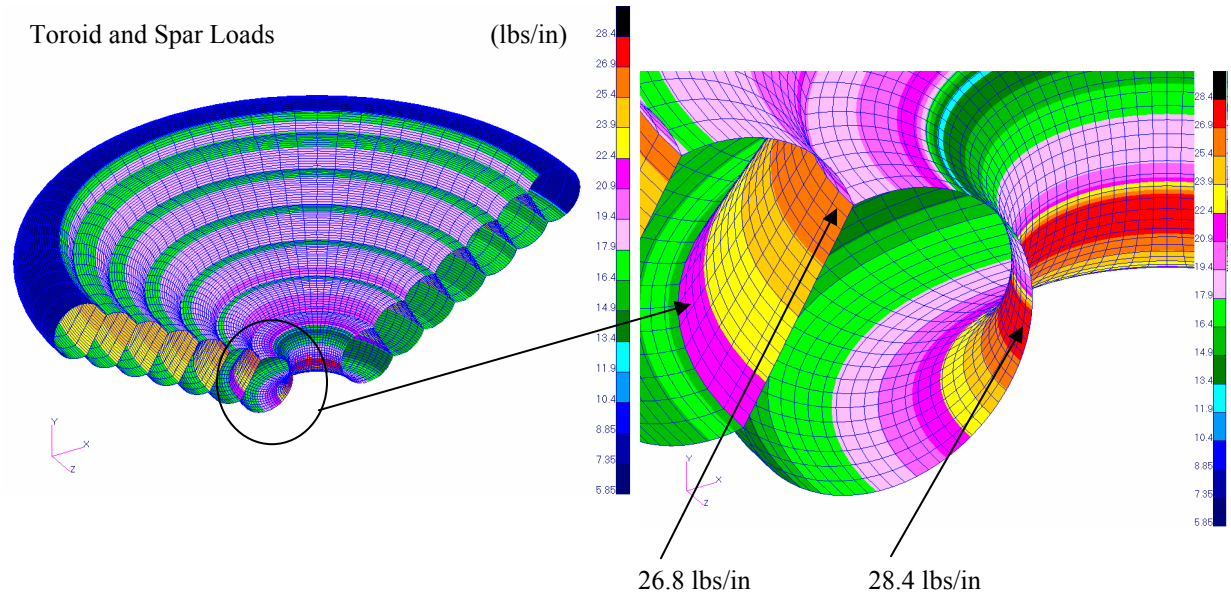

Figure 8. Meridional shell force resultants in the toroids and spars.

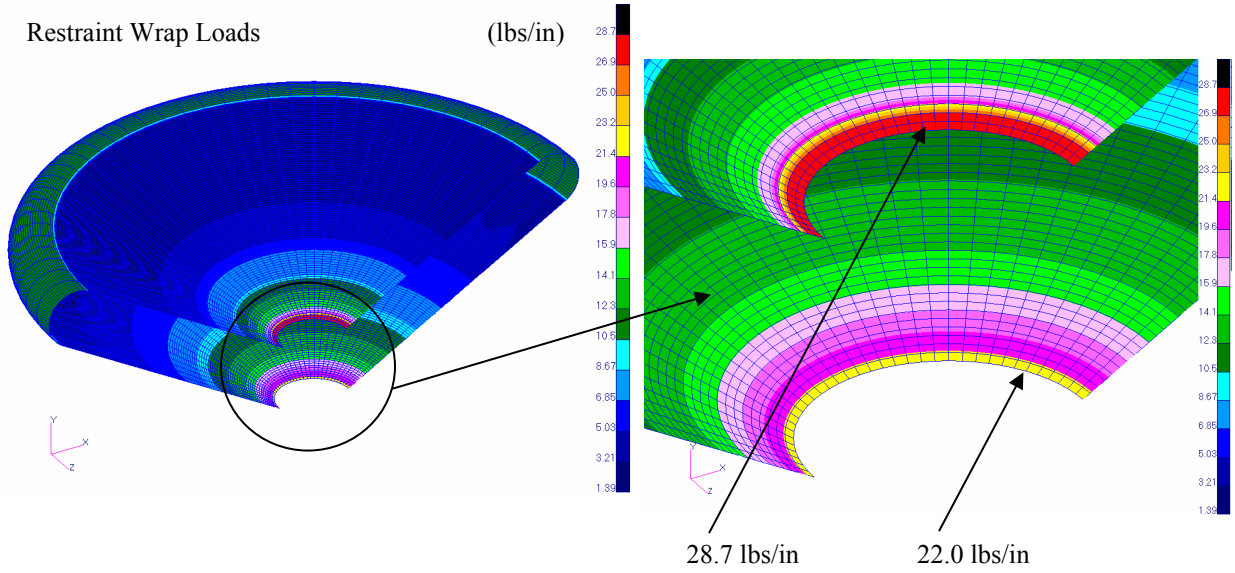

Figure 9. Meridional shell force resultants in the restraint wrap.

5. Thermal Considerations

The operating temperatures of the aeroshell layers were important for material selection as well as for seam constructions. The maximum temperature occurs on the outermost windward layer, decreasing as it passes through subsequent layers. The maximum temperature on the outermost windward layer is predicted to be 274°C, decreasing to 186°C at the windward restraint wrap.

C. Fabric Material Testing

1. Physical Property Testing

There are two base fabrics selected for the aeroshell bladder material. Both materials consist of a Kevlar base cloth; the bladder gore patterns are silicone coated while the spars remain uncoated. The inner two toroids and spars are constructed from a more robust/heavier Kevlar base cloth since they see the highest skin stresses due to inflation pressure. As a mass savings approach, the outer two volumes were constructed from a lighter weight Kevlar fabric capable of carrying the lower skin stresses. The silicone coating is applied to the base cloth only as a gas retention layer; it does not contribute to the fabric strength. Traditional uni-axial strength results were obtained for both of the bladder materials at both room temperature and the predicted operating temperature during reentry. The properties of the structural layers at elevated temperatures was of particular importance since reduction of the tensile strength was expected given that Kevlar fabric begins to decompose at high temperatures (427°C – 482°C). The properties of the two bladder fabrics at room temperature are shown in Table 2.

Table 2. Bladder material physical properties

Property	Inner Two Toroids	Outer Five Toroids	Spars
	23°C	**23°C**	**23°C**
Weight (oz/yd^2)	11.2	6.6	5.8
Thickness (mils)	13.7	8.0	10.0
Tensile Strength (lbs/in)	756	258	962
Tear Strength (lbs)	698	156	689

Strong adhesion of the silicone coating to the Kevlar base fabric is important to ensure optimal performance with respect to both gas retention and adhesion of reinforcements. Therefore each coated Kevlar fabric was subjected to peel adhesion testing in operational configurations to confirm sufficient coating adhesion was obtained. In all instances, excellent peel strength was obtained, greater than 10 lbs/in.

The structural restraint wrap consists of two layers of uncoated Kevlar fabric. This Kevlar fabric is the same base cloth used for the bladder layer of the outer five toroids. The room temperature properties of the restraint wrap (single layer) are given in Table 3.

Table 3. Restraint material physical properties

Property	Restraint Wrap
	23°C
Weight (oz/yd^2)	2.1
Thickness (mils)	5.0
Tensile Strength (lbs/in)	358
Tear Strength (lbs)	160

2. Bi-axial Testing

Using a bi-axial test methodology, ILC Dover quantified the response of the selected Kevlar fabrics subjected to bi-axial load conditions (Fig. 10). Bi-axial loads are typical for orthogonally constructed fabric in an inflated structure.

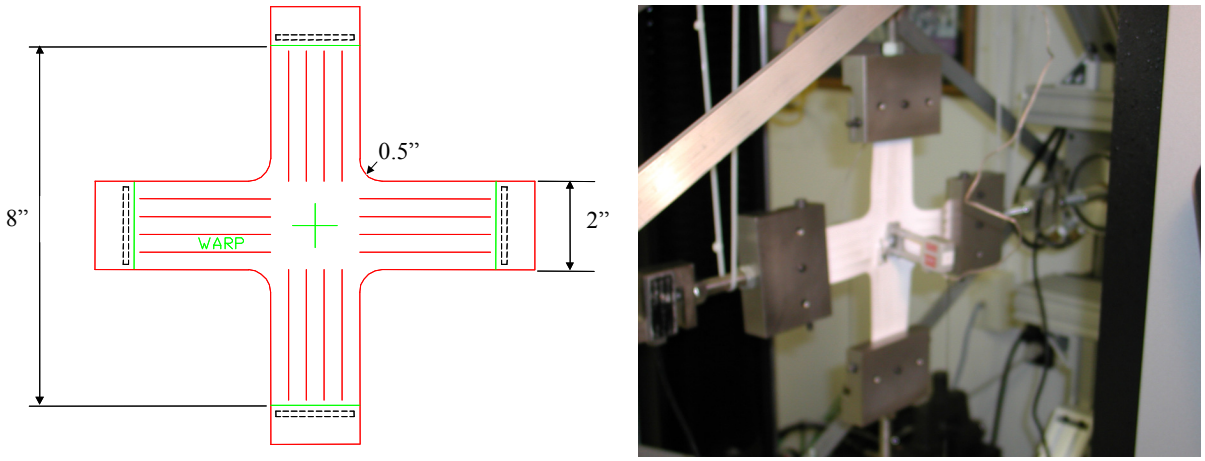

Figure 10. Bi-Axial material testing apparatus.

The results of this testing have proven to contribute highly accurate material properties for analysis compared to traditional uni-axial approaches. The difference between these methodologies has been demonstrated on IRVE and is represented by the IRVE restraint material results shown in Fig. 11.

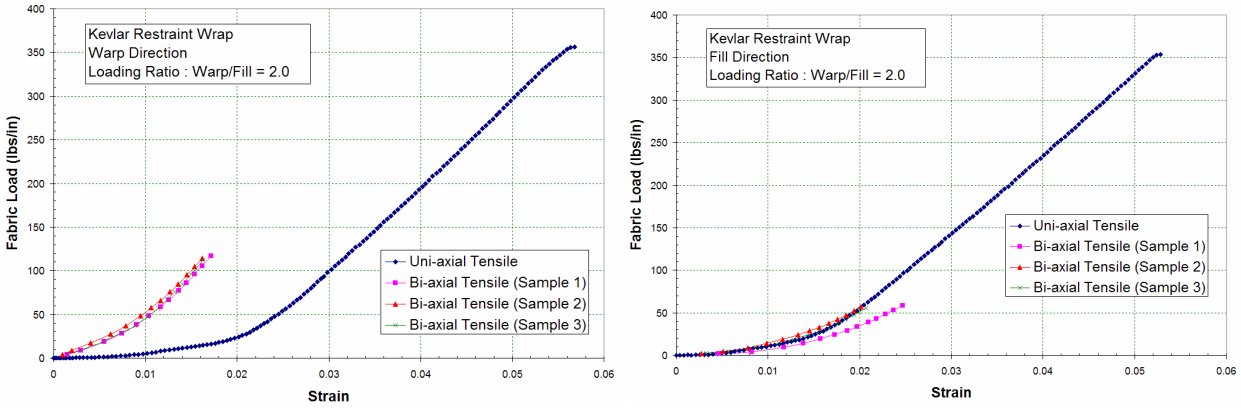

Figure 11. IRVE bi-axial test results on the restraint material.

These results can be used to resize patterns to account for material elongation, which results in increased accuracy of the inflatable, and as an input into structural analysis and impact analysis, which allows for higher accuracy in shape and load prediction.

3. Seam Testing

Sewn and taped seams are used to join the various patterns together as they approximate the 3-dimensional shape of the IRVE aeroshell. The seams are defined by their combination of fabric layers, stitch count, stitch type, number of stitch rows, and thread. A variety of potential seam constructions were evaluated to determine the optimum construction for each material and application.

The IRVE aeroshell employs several different seam constructions and attachment techniques for various components. The primary seam that joins the bladder and the restraint gores is a 0.5-inch wide fell seam. The attachment employs a 0.5-inch seam construction joined to a continuous T-tape, which spans the bladder join seams. The tested strengths of the bladder seams at room temperature are listed in Table 4. Both the bladder join seams and the spar attachment have a non-reinforced silicone film tape applied to them to reduce leakage to a level that can be maintained by the inflation system and sustain the required pressure as the inflatable passes through the peak pressure pulse.

Table 4. Bladder seam strengths

Seam Type	Required Strength at Proof Pressure (lbs/in)	Required Strength at Entry (lbs/in)	Tested Results (lbs/in)	Margin of Proof Test at 23°C
			23°C	
Join Seam – Inner Two Toroids	49	28	348	7.1
Join Seam – Outer Five Toroids	49	28	275	5.6
Spar Seam – Inner Two Toroids	101	67	318	3.1
Spar Seam – Outer Five Toroids	101	67	330	3.3

The restraint seam constructions of particular importance are the attachments to the centerbody since these locations carry the majority of the entry loads. The restraint attaches to the windward side of the centerbody with a clamped deadman interface and to the leeward side with a cord laced attachment (Fig. 12).

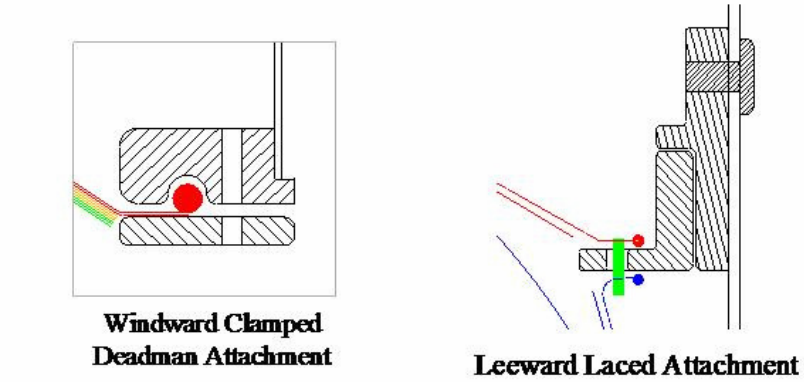

Figure 12. Restraint attachment designs.

The tested strengths of the restraint seams at room temperature are listed in Table 5.

Table 5. Restraint seam strengths

Seam Type	Required Strength at Proof Pressure (lbs/in)	Required Strength at Entry (lbs/in)	Tested Results (lbs/in)	Margin of Proof Test at 23°C
			23°C	
Join Seam	8.5	8.5	324	38.1
Windward Attachment	8.0	28.7	284	35.6
Leeward Attachment	6.75	22.0	366	54.2

The Kapton and Nextel seams require minimal strength since the Kevlar restraint carries the loads from reentry and inflation. However the seams' integrity during packing, deployment and entry is important in order to properly maintain the thermal protection. It is also of particular importance for the outermost Nextel layer to maintain as smooth a surface as possible so as not to create thermal hot spots. The Kapton patterns are joined together with a butt and taped seam. Since the surface profile of the outermost Nextel layer is so important, there are two seam constructions used to join the Nextel patterns. The outer layer's 1.0-inch pinched and turned seam presents a smother profile than inner layer's 1.0-inch lap seam construction. Table 6 contains the results of the seam testing of the insulation materials.

Table 6. Insulation seam strengths

Seam Type	Required Strength (lbs/in)	Tested Results (lbs/in)
		23°C
Kapton Radial Seam	Minimal required	73.2
Seam Type	**Required Strength (lbs/in)**	**Tested Results (lbs/in)**
		23°C
Nextel Outer Seam	Minimal required	37
Nextel Inner Seam	Minimal required	48

V. Inflatable Aeroshell Fabrication

A. Inflatable Shape Accuracy

Shape definition of the inflatable structure is the result of 3-D modeling of the aeroshell system using PTC Pro/Engineer. This model is used to define patterns to reproduce the desired geometry of the aeroshell structure (Fig. 13). The patterning takes into account the net material dimensions after the inflation load is applied. The material properties obtained during the bi-axial testing, such as bi-axial modulus, are also considered during pattern definition along with the seam construction.

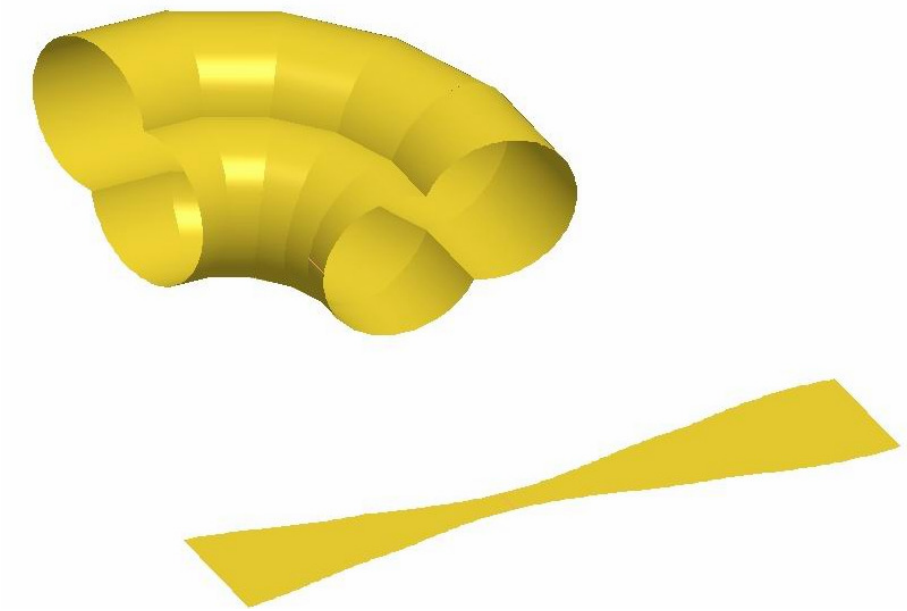

Figure 13. IRVE 3-D model of an inflatable component with raw flat pattern layout.

To further support the development of the IRVE inflatable design, a full-scale prototype unit was constructed to validate the shape of the inflated structure. Photogrammetry equipment is used to characterize the static shape after inflation. By triangulating from known camera positions to the location of identical targets on a series of photographs, a three dimensional model of an imaged surface can be obtained. Photogrammetry results of the bladder were used to verify the patterned geometry met the accuracy requirements of the IRVE aeroshell system (Fig. 14). The results can also be used as an "as-manufactured" aeroshell geometry model for aerodynamic, thermal and structural analyses to define shape tolerance and secure mission success for the flight system.

Figure 14. IRVE full-scale prototype system surface (grey) vs. nominal required shape (blue).

B. Inflatable Aeroshell Validation and Testing

All inflatable components that are assembled for testing or flight will be tested for design conformance prior to use. In addition to specific design aspects such as packing and deployment, inflatable envelopes are subjected to a leakage test to evaluate the system gas losses, then subjected to an over-pressure test to certify design safety margin, construction and workmanship, and subjected to a final leakage to quantify delivered performance and preclude damage due to over-pressure testing.

VI. Development Unit Stiffness/Dynamics Test

Prior to construction of a full-size aeroshell, ILC Dover constructed a smaller, two-cell demonstration unit (approximately 48 inches in diameter) to demonstrate fabrication techniques and assembly, and to provide NASA Langley with a unit to test for stiffness and dynamics for the purpose of finite element model correlation. A series of static and dynamic tests were performed to measure the stiffness of the inflated article. The stiffness tests consisted of hanging a series of increasing weights to one side of the aeroshell and measuring the displacements at several locations. After the final weight was added and displacements recorded the weights were suddenly removed by cutting a string supporting the weights and the resulting dynamic decay response was measured with a laser vibrometer. These tests were repeated for a series of inflation pressures ranging from 1.0 to 3.0 psi. The test setup is shown in Fig. 15. Load/deflection curves from the 3.0 psi (flight pressure) test are shown in Fig. 16. The time traces for the dynamic responses at the various inflation pressures are shown in Fig. 17. Data from both the static and dynamic tests were used to update the finite element model material properties. The updated properties were then used in the flight finite element model to predict the expected fundamental mode during free flight. The fundamental mode of the flight system was calculated to be 6.0 Hz.

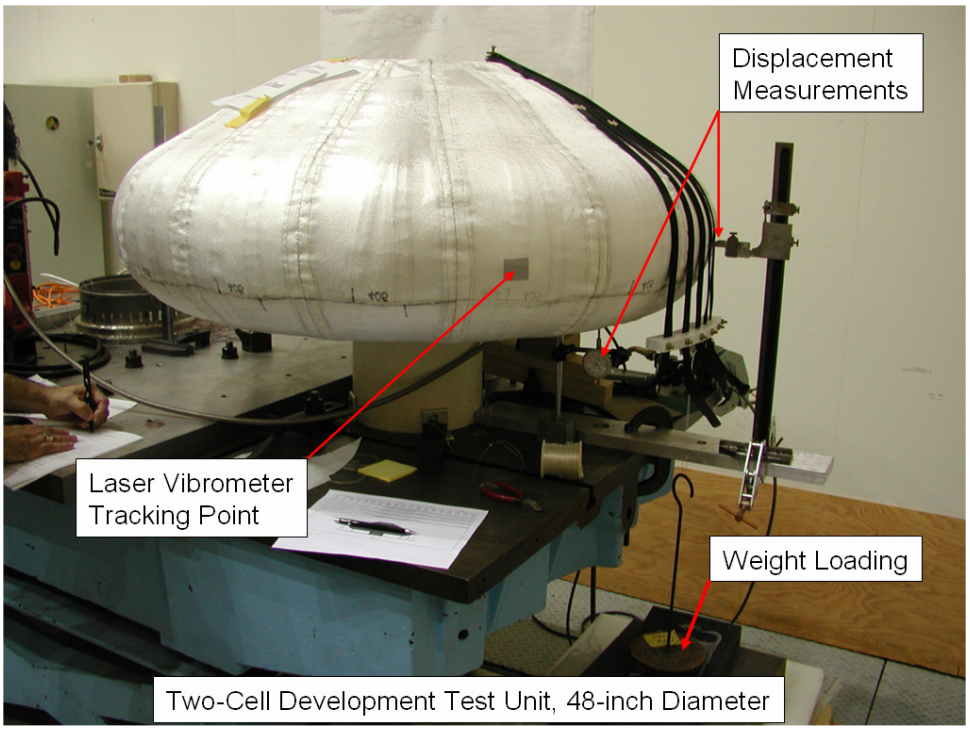

Figure 15. Test setup for the development test unit.

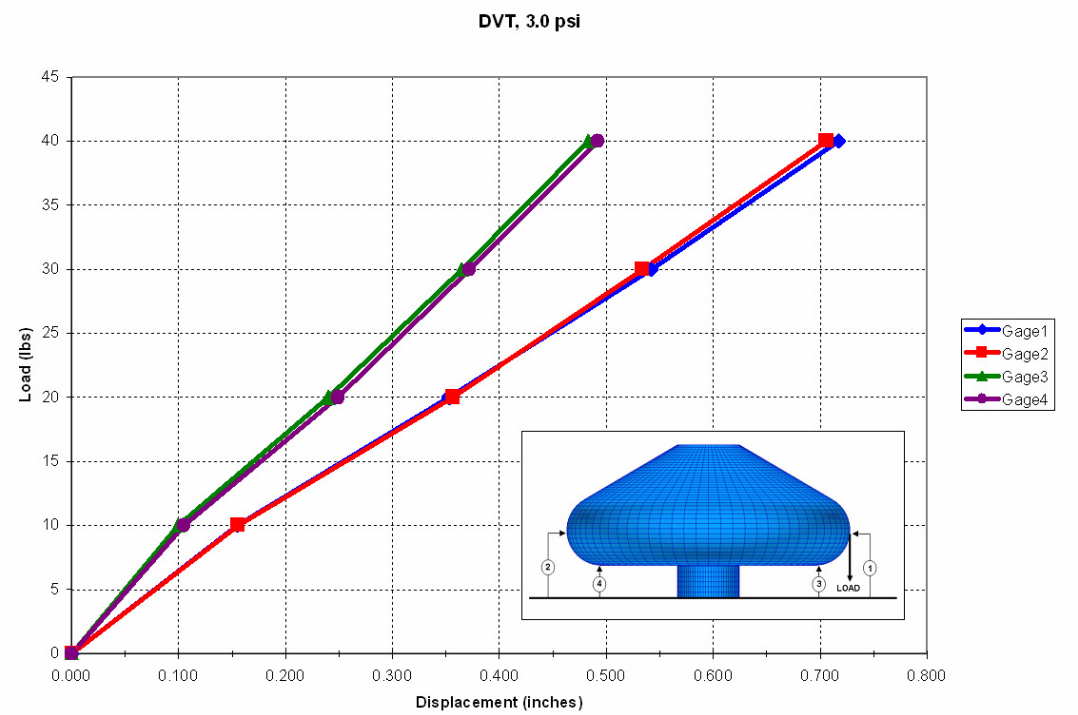

Figure 16. Load/deflection curves at inflation pressure of 3.0 psi.

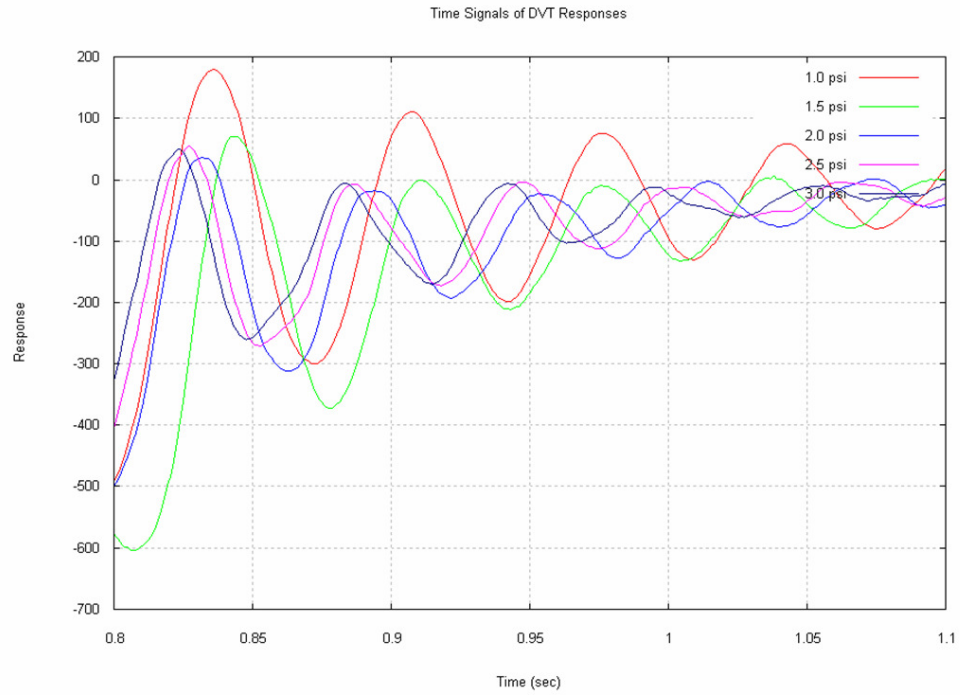

Figure 17. Dynamic responses from the demonstration unit tests.

VII. Vacuum Modal Survey Test

Following the demonstration unit, a full-scale prototype unit was built by ILC Dover and delivered to NASA Langley for deployment testing, leak testing, and modal survey testing. The centerbody structure was a plastic mock-up of the actual centerbody outer geometry. The test setup is shown in Fig. 18.

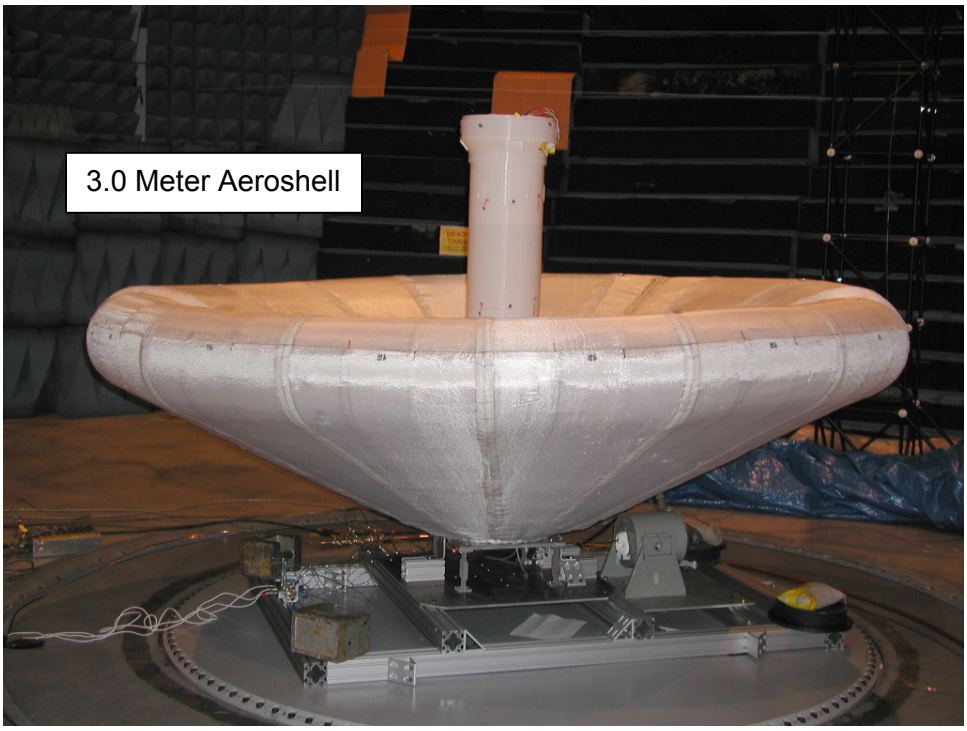

Figure 18. Test setup for the vacuum modal survey.

The test was conducted in a 16-meter vacuum sphere, where the pressure was held at about 0.25 torr. For the modal survey, a 25-lb shaker was attached to a flexible mounting system for the IRVE assembly. The shaker and flex mount support structure are shown in Fig. 19. A laser vibrometer system, located outside the chamber, was used to measure the dynamic response. The laser was fired through a window in the chamber and directed to targets by a mirror system. The targets were placed around the rim and at the top of the centerbody as shown in Fig. 20.

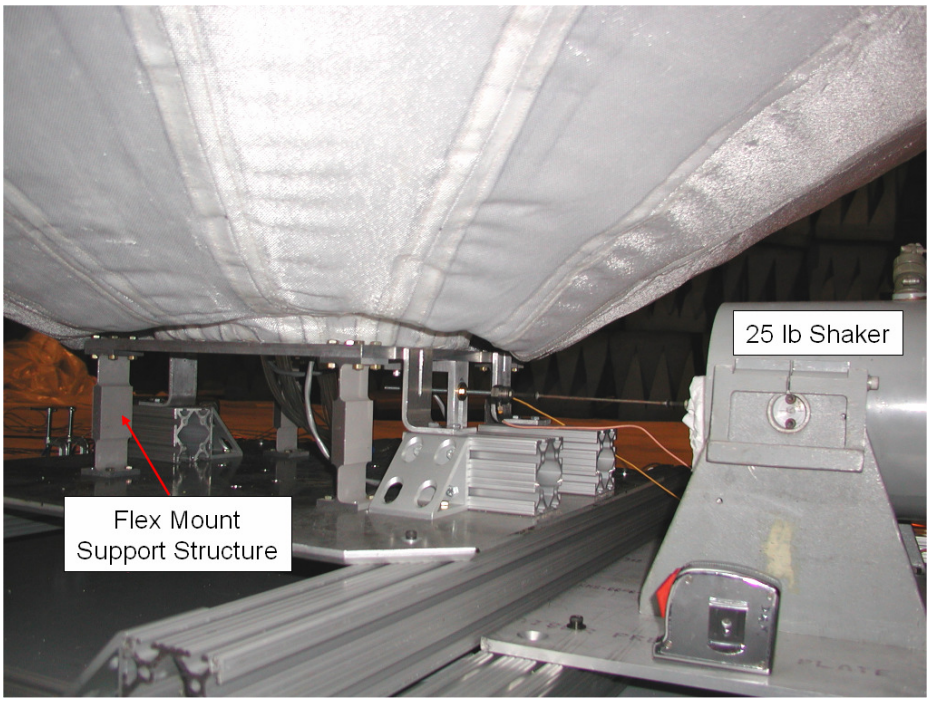

Figure 19. Shaker and flex mount support structure.

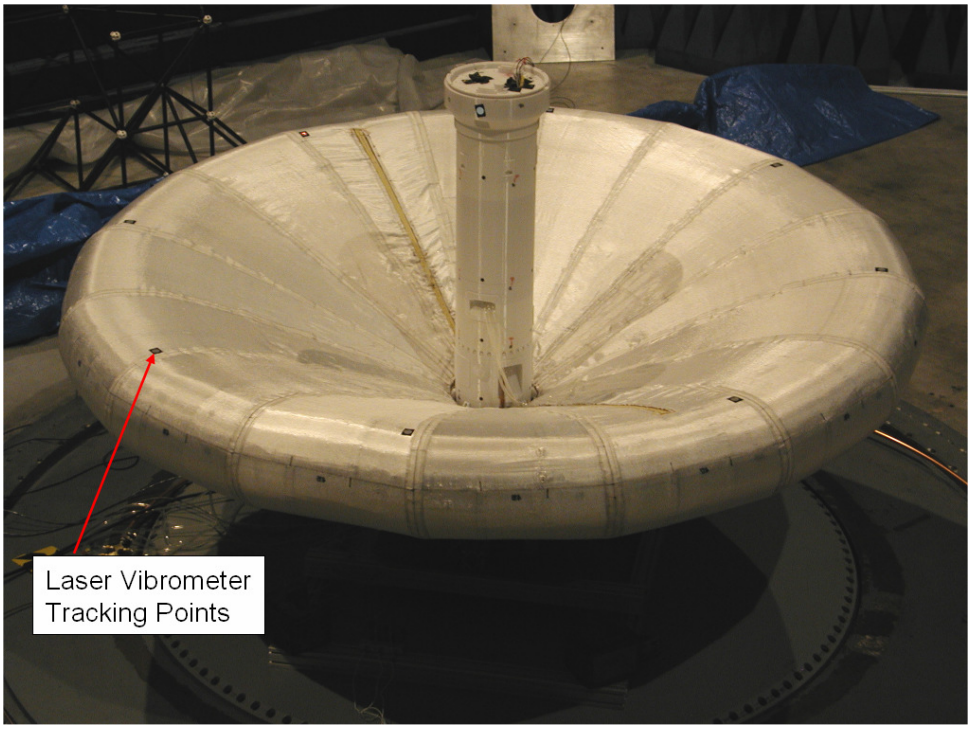

Figure 20. Laser vibrometer tracking points.

The finite element model for the modal survey is shown in Fig. 21. A separate test was conducted on the flex mount support structure to verify its dynamic behavior. Once the system frequencies were determined the fabric material properties were adjusted resulting in the test/analysis correlation shown in Table 7.

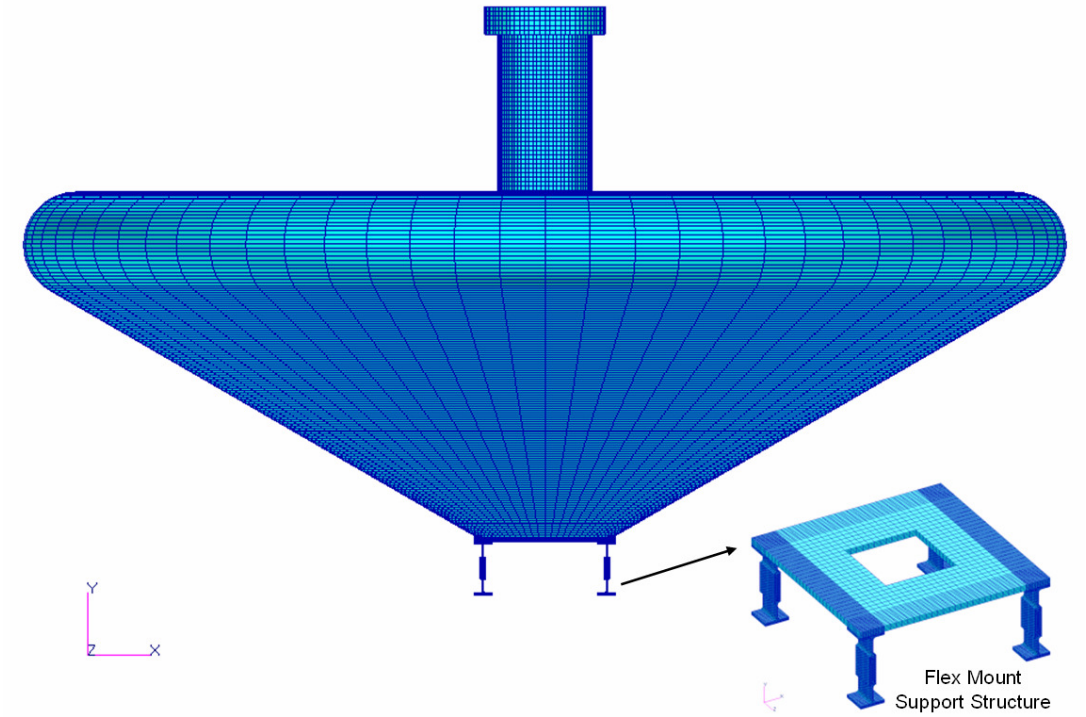

Figure 21. Finite element model for the modal survey test.

Table 7. Test/analysis frequency correlation

Mode	Test Frequency (Hz)	Analysis Frequency (Hz)	% Difference
1 – Fundmental Rocking Mode of Inflatable	3.31	3.47	4.8
2 – Fundamental Rocking Mode of Inflatable	3.52	3.53	0.3
3 – Support Flexing + Inflatable Rocking	7.7	7.68	-0.3
4 – Bounce Mode of Inflatable	11.8	11.47	-2.8

The correlated material properties were then incorporated into the flight finite element model and a modal analysis was run in the free-free (in-flight) condition under inflation pressure alone and with external aerodynamic pressure added. The predicted in-flight fundament mode is shown in Fig. 22. The minimum frequency is expected to be 6.7 Hz, which is sufficiently above the expected aerodynamic excitation force frequency range (< 1 Hz). During flight this mode will be monitored with photogrammetric measurements of the leeward side of the aeroshell.

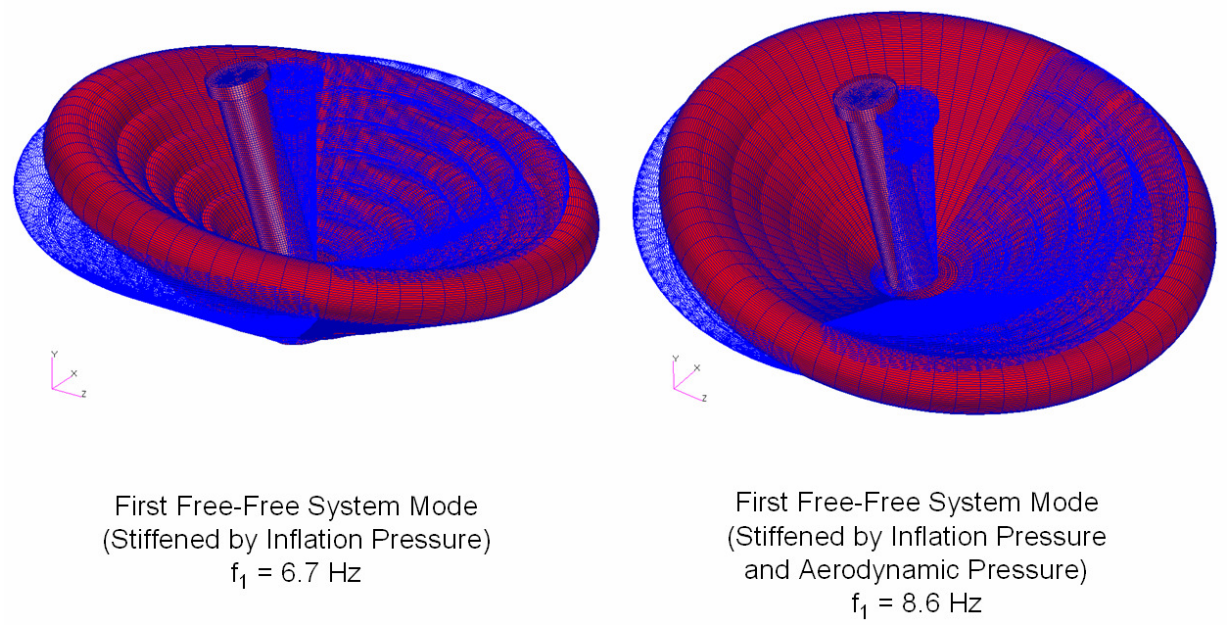

Figure 22. Predicted in-flight fundamental mode.

VIII. Conclusion

The IRVE inflatable structure has been analyzed and tested. Structural loads are well within the capability of the fabrics selected, with the highest fabric loads occurring in the spars due to stress concentration effects. Closed-form equations can be used to accurately predict nominal loads in the fabric structures without detailed finite element analyses. Fabric material testing provided initial values of elastic moduli to use in finite element models and subsequent static and dynamic testing of inflated assemblies refined the moduli for expected flight conditions. Finite element models using the updated material properties were then used to predict the fundamental mode of the inflatable aeroshell during free flight. The fundamental mode is expected to be sufficiently above the aerodynamic excitation forces so as not to cause aerodynamic instabilities.

Acknowledgments

The authors would like to acknowledge the efforts of the entire IRVE team at NASA Langley Research Center, NASA Wallops Flight Facility, and ILC Dover for bringing this experiment to fruition. Special thanks to Troy Mann of the Structural Dynamics Branch (Swales Aerospace) at NASA Langley who conducted the prototype modal survey.

References

[1]Hughes, S. J., Dillman, R. A., Starr, B. R., Stephan, R. A., Lindell, M. C., Player, C. J., and Cheatwood, F. M., "Inflatable Re-entry Vehicle Experiment (IRVE) Design Overview," AIAA Paper AIAA 2005-1636, 18th AIAA Aerodynamic Decelerator Systems Technology Conference and Seminar, Munich, Germany, May 23-26, 2005.

[2]Player, C. J., Cheatwood, F. M., and Corliss, J., "Development of Inflatable Entry Systems Technologies," 3rd International Planetary Probe Workshop, Anavyssos, Greece, June 27-July 1, 2005.

[3]Starr, B. R., Bose, D. M., Thornblom, M., and Kilcoyne, D. "Inflatable Reentry Vehicle Experiment Flight Performance Simulations," 53rd JANNAF Propulsion Meeting, Monterey, CA, Dec. 5-8, 2005.